Comparison and Extension of Existing 3D Propagation Models with Real-World Effects Based on Ray-Tracing

A Basis for Network Planning and Optimization

Dereje W. Kifle · Lucas C. Gimenez · Bernhard Wegmann · Ingo Viering · Anja Klein

Abstract The next generation of cellular network deployment is heterogeneous and temporally changing in order to follow the coverage and capacity needs. Active Antenna Systems allows fast deployment changes by cell shaping and tilt adaptation which have to be controlled in self-organized manner. However, such kind of automated and flexible network operations require a Self Organizing Network (SON) algorithm that works based on network performance parameters being partly derived from the radio measurements. Thus, appropriate radio propagation models are not only needed for network planning tools but also for simulative lab tests of the developed SON algorithm controlling the flexible deployment changes enabled by Active Antenna Systems. In this paper, an extension of the existing 3D propagation model is proposed in order to incorporate the propagation condition variation effects, not considered so far, by changing antenna beam orientation like antenna tilting or when users are distributed in the third dimension (height) in multi-floor scenarios. Ray tracing based generated propagation maps that show the realistic propagation effect are used as 3D real world reference for investigation and model approval.

D. W. Kifle (✉) · B. Wegman
Nokia Solutions and Networks, Munich, Germany
e-mail: dereje.woldemedhin.ext@nsn.com

B. Wegman
e-mail: bernhard.wegmann@nsn.com

L. C. Gimenez
Aalborg University, Aalborg, Denmark
e-mail: lcg@es.aau.dk

I. Viering
Nomor Research GmbH, Munich, Germany
e-mail: viering@nomor.de

A. Klein
Technische Universität Darmstadt Communications Engineering Lab, Darmstadt, Germany
e-mail: a.klein@nt.tu-darmstadt.de

 Springer

Keywords Propagation model · Shadowing · Antenna tilt

1 Introduction

Cellular system design requires an in depth understanding of the characteristics of the propagation environment. Therefore, accurate and robust propagation prediction models are needed to be able to predict the characteristics of the physical radio channel where the cellular system is going to be deployed. A very good prediction of the radio channel ensures more reliability in delivering high system capacity with high efficiency and provides more flexibility in further optimization. As the impact of the propagation environment is determined by several factors, including the operating frequency of the radio signal and varying clutter type, its modeling is the most difficult task. Plenty of propagation models and prediction schemes have been proposed for various case scenarios and are being utilized in order to approximate all those effects and predict the signal power loss in the course of propagation [1–4].

The total propagation loss of a signal can be modeled as a distance dependent path loss plus an additional random variable component which depends on the nature of the propagation environment characteristics. The path loss component $L(\overline{x})$, also known as distance dependent path loss, gives the average signal attenuation level and it is exponentially proportional to the shortest distance r between the receiver terminal location $\overline{x}$ and the transmitter antenna, $L \propto r^{\beta}$, where β is called the path loss component and its value depends on the clutter type of the propagation environment in the vicinity of the receiving mobile terminal, such as terrain, buildings, vegetation, etc. Different kinds of path loss models are available in literatures that are derived based on analytical and empirical approaches [2,3]. The additional variability of the propagation loss component is caused by different physical phenomena that the radio wave undergoes in the course of propagation, i.e. reflection, diffraction and scattering thereby resulting in a signal fading. The large scale signal fading which is known as shadowing is typically modeled as a random variation of a signal attenuation level around the path loss caused by presence of obstructing objects on the path of the signal propagation [5,6] and therefore, it is location dependent.

Proper radio propagation models are not only needed for network planning tools but also in system level simulators being used to evaluate Self Organizing Network (SON) algorithms designed for flexible deployment changes enabled by Active Antenna Systems (AAS). Antenna beam characteristics can be fast adapted from simple tilt changes to more complicated beam shaping techniques like cell splitting [7]. Such types of network operation changes are implemented in a system level simulator or network planning tool where the prediction of the expected network performance indicators like coverage, signal to interference level, etc. are calculated by utilizing propagation models [6]. Hence, accurate propagation model that is able to reflect a very good approximation of the realistic propagation effect is essential. The existing models and assumptions are fair enough for application as used in network planning tasks for stationary deployments. However, automated traffic dependent network adaptation and optimization of the 3D antenna characteristics require an accurate approximation of the realistic propagation condition. Due to this fact, the performance of such algorithm later in the field is limited by the accuracy of the utilized models during the development of the algorithm.

Shadowing effect is modeled as a log-normal distributed random variable with zero mean and a standard deviation of 5–12 dB depending on the nature of the propagation environment. Shadowing is assumed to be a Gaussian process that de-correlates exponentially with distance and its value is assumed to be constant at a fixed location as long as deployment is not changed

[5,6]. However, when the antenna beam orientation is changed, the radio signal experiences a different propagation behavior for the same user location resulting from changed path way of the radio wave. The received signal change does not only result from changing antenna beam direction but also from a change in shadowing effect [5,6]. This variability of the shadowing and its dependency with respect to antenna tilt changes are presented in [8]. Their effect requires, therefore, a new shadowing model taking the tilt dependency into account.

This paper provides more further studies of the shadowing effect variability with respect to antenna tilt changes which are used as basis to introduce a new shadowing model. The tilt dependency of the shadowing process is statistically approximated based on the propagation statistics generated using a ray tracing based network planning tool that employs 3D model for a typical European urban deployment scenario. Moreover, the paper also investigates the height gain variation in the propagation loss associated to different clutter type experience for a signal at a different height level. This height gain effect becomes necessary when considering in-door users in multi-floor building scenarios. Thus a height dependent propagation model is also presented utilizing ray tracing based propagation maps generated at different floor height levels.

The paper is organized as follows: Sect. 2 formulates the problem and the proposed propagation models are presented in Sect. 3. The scenario description, site layout and other settings used in the ray tracing tool are described in Sect. 4. Section 5 discusses and evaluates the performance of the proposed models using propagation statistics from ray tracing. The impact of the tilt and height models in planning and optimization is discussed in Sects. 6 and 7 concludes the work.

2 Problem Formulation

2.1 Tilt Dependency of Propagation Model

Assuming the antenna beam has a tilt setting of Θ_o, a pixel point in a network located at $\overline{x}$ and at a height of h_o above the ground with respect to the base station antenna, i.e. $\overline{x}_{h_o}$, the total propagation loss from the transmitting antenna to $\overline{x}_{h_o}$ is described by $L_t(\overline{x}_{h_o}, \Theta_o)$. In the existing propagation model [6], the $L_t(\overline{x}_{h_o}, \Theta_o)$ is given by:

$$L_t(\overline{x}_{h_o}, \Theta_o) = L(\overline{x}_{h_o}) - G_a(\overline{x}_{h_o}, \Theta_o) + S(\overline{x}_{h_o}) \qquad (1)$$

where $L(\overline{x}_{h_o})$ is the distance dependent path loss and $S(\overline{x}_{h_o})$ is a log-normal random variable with zero mean and standard deviation of σ, $S(\overline{x}_{h_o}) \sim \mathcal{N}(0, \sigma^2)$, that gives the shadowing fading effect. The term $G_a(\overline{x}_{h_o}, \Theta_o)$ is the total antenna gain at $\overline{x}_{h_o}$ and it is given by the sum of the dBi gain of the antenna A_{dBi} and the three dimensional radiation pattern loss $B_p(\Phi, \Theta_o, \phi, \theta)$ normalized to the maximum antenna gain value and given in terms of the azimuth and elevation angular location of $\overline{x}_{h_o}$, (ϕ, θ), the antenna beam azimuth orientation Φ and the elevation tilt Θ_o: i.e. $G_a(\overline{x}_{h_o}, \Theta_o) = A_{dBi} + B_p(\Phi, \Theta_o, \phi, \theta)$.

When the elevation tilt configuration is changed from Θ_o to Θ_i the total propagation loss at $\overline{x}_{h_o}$ with respect to the new tilt configuration Θ_i, $L_t(\overline{x}_{h_o}, \Theta_i)$, is described by the existing model [6] as shown in Eq. (2).

$$L_t(\overline{x}_{h_o}, \Theta_i) = L(\overline{x}_{h_o}) - G_a(\overline{x}_{h_o}, \Theta_i) + S(\overline{x}_{h_o}) \qquad (2)$$

According to the model, the associated change in the total propagation loss while the tilt configuration is changed is described by only the difference in the total antenna gain value $\Delta G_a(\overline{x}_{h_o}, \Theta_i, \Theta_o)$ experienced at the same location before and after applying the tilt change
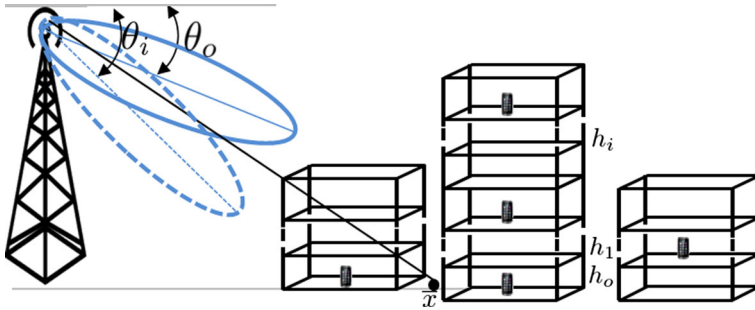
Fig. 1 Different tilt settings and multi-floor propagation scenario

where $\Delta G_a(\overline{x}_{h_o}, \Theta_i, \Theta_o) = G_a(\overline{x}_{h_o}, \Theta_i) - G_a(\overline{x}_{h_o}, \Theta_o)$. Whereas the $L(\overline{x}_{h_o})$ is not affected as it is dependent only on the distance r and the shadowing effect is assumed to be identical and, hence, always the same shadowing is assumed independent of the tilt. Accordingly, the total propagation loss after a tilt change is expressed in terms of the total propagation loss before the change and the difference in the total antenna gain at $\overline{x}_{h_o}$ associated to the applied tilt change in Eq. (3):

$$L_t(\overline{x}_{h_o}, \Theta_i) = L_t(\overline{x}_{h_o}, \Theta_o) + \Delta G_a(\overline{x}_{h_o}, \Theta_i, \Theta_o) \tag{3}$$

However, in reality, in the presence of obstructing building environments, the shadowing effect does not remain identical during tilt configuration change. The variability of the shadowing with respect to tilt change has been shown by extracting shadowing maps from propagation maps generated using a ray tracing tool that reflects the real propagation effect changes by employing a ray based prediction in a real based 3D model scenario in [8]. The ray tracing scenario and further scenario description are discussed in the forthcoming sections. Based on the ray tracing based generated propagation maps, it has been observed that the total propagation loss change during a tilt change is not equal to only the total antenna gain difference as described in the existing model in Eq. (3) but also on the shadowing effect change associated with the applied tilt difference. The paper [8] discusses the impact of tilt change on the shadowing value and the result shows the existence of dependency of the shadowing with the tilt configuration setting. However, in [8], only the impact of tilt setting on propagation shadowing is discussed. Therefore, tilt dependent shadowing model denoted by $S(\overline{x}_{h_o}, \Theta_i)$ is required in order to properly include the shadowing effect change while carrying out tilt related system level simulation. As a consequence, an enhancement of the existing shadowing model is proposed to include propagation effect variation with tilt configuration change.

2.2 Height Gain

In urban areas with high rise buildings, mobile users are probably distributed at different height levels above the ground on various building floors as depicted in Fig. 1. For a multi-floor building scenario, the prediction of the total propagation loss for indoor users residing at different floors requires proper approximation of the outdoor propagation and the corresponding penetration loss. In many existing planning tools and models, the common approach to estimate the indoor propagation loss is to predict the outdoor propagation loss in the proximity of the buildings and then add some additional constant penetration loss [9,10]. The corresponding outdoor propagation conditions are also dependent on the surrounding clut-

ter type projected from the corresponding floor height level. Apparently, at a higher height levels, the clutter type gets better leading to a higher probability of line of sight visibility between the transmitter and the receiver. Consequently, this clutter level variation leads to a propagation gain with height. The existing propagation model approximates a so-called a floor height gain $H(\overline{x}_{h_i,h_o})$ which is included when the height level changes from h_o to h_i. Hence, the existing model prediction of the total propagation loss $L_t(\overline{x}_{h_i}, \Theta_o)$ at h_i height level is done by applying the floor height gain to the the total propagation loss at h_o as shown in Eq. (5)

$$L_t(\overline{x}_{h_i}, \Theta_o) = L_t(\overline{x}_{h_o}, \Theta_o) + H(\overline{x}_{h_i,h_o}) \tag{4}$$

In the existing models [9,10], $H(\overline{x}_{h_i,h_o})$ is accounted and approximated with a constant average floor height gain values determined from different measurement statistics. In COST 231 [10], floor height gain of 1.5–2 dB/floor and 4–7 dB/floor has been reported for buildings with storey heights of 3 and 4–5 m respectively. The floor height gains are translated to dB/m to be generally applied for floors with different floor height. Currently, an average height gain of 0.6 dB/m is proposed by COST and is widely adopted in different literatures [9,10]. The studies in [9] have also indicated that this value of 0.6 dB/m is independent of the operating frequency and the relative distance from the corresponding base station.

However, since all these models recommend constant floor height gain values independent of the type of the building scenario, in some cases, this does not properly reflect the actual gain variation per height relative to what is assumed at the ground level. Hence, enhanced height gain model that includes the floor height gain variation with respect to the ground floor is required to better reflect the non constant height gain level in order to be able to predict the propagation loss accurately when dealing with a multi-floor building scenario in network planning and system level simulation setups.

3 Derivation of Tilt and Height Dependent Propagation Model

3.1 Tilt Dependent Shadowing Model

Antenna tilt configuration change from Θ_o to Θ_i is primarily intended to change the cell coverage by directing the beam orientation in a desired direction in order to have change in the total antenna gain with respect to each location $\overline{x}_{h_o}$ in a network. During the tilt adjustment, the path loss component, however, is not affected due to the fact that it is rather dependent only on the relative distance of $\overline{x}_{h_o}$ from the base station.

As stated in Sect. 2.1, the tilt setting change has an impact on the shadowing effect of the propagation environment, particularly, in urban clutter type case. Thus, shadowing at a tilt Θ is modeled as tilt dependent, $S(\overline{x}_{h_o}, \Theta)$. In our extended shadowing model derivation, tilt specific shadowing values, $S(\overline{x}_{h_o}, \Theta)$, are extracted from propagation maps generated with a ray tracing tool at various Θ settings. Hence, a new propagation model is required where the effect of the experienced change in the shadowing $\Delta S(\overline{x}_{h_o}, \Theta_i, \Theta_o)$ is considered in case of tilt configuration changes, $\Delta S(\overline{x}_{h_o}, \Theta_i, \Theta_o) = S(\overline{x}_{h_o}, \Theta_i) - S(\overline{x}_{h_o}, \Theta_o)$, accordingly, the new total propagation loss $\hat{L}_t(\overline{x}_{h_o}, \Theta_i)$ that includes tilt dependent shadowing variation after tilt change from Θ_i to Θ_o can be expressed as shown in Eq. (5).

$$\hat{L}_t(\overline{x}_{h_o}, \Theta_i) = L_t(\overline{x}_{h_o}, \Theta_o) + \Delta G_a(\overline{x}_{h_o}, \Theta_i, \Theta_o) + \Delta S(\overline{x}_{h_o}, \Theta_i, \Theta_o) \tag{5}$$

Since the shadowing process is modeled as log-normally distributed random value, the shadowing difference, $\Delta S(\overline{x}_{h_o}, \Theta_i, \Theta_o)$, can be also approximated to follow a log-normal

distribution with zero mean and a standard deviation of $\sigma_{\Delta S}$. It has been found from ray tracing based data, to be discussed more in later section, that with the tilt configuration change, $\Delta\Theta = \Theta_i - \Theta_o$, the shadowing effect experience for a user at $\overline{x}_{h_o}$ becomes more different and the random shadowing values become more and more de-correlated at a higher $\Delta\Theta$. The statistical correlation between the random shadowing values at $\overline{x}_{h_o}$ at two different settings, Θ_i and Θ_o is given by the correlation coefficient value $\rho^{\Theta_i\Theta_o}$ and the respective tilt shadowing statistics are assumed as a zero mean, $\mu_{\Theta_i} = 0$. The correlation coefficient is given by:

$$\rho^{\Theta_i\Theta_o} = \frac{\mathrm{Exp}\{(S(\overline{x}_{h_o}, \Theta_i) - \mu_{\Theta_i})(S(\overline{x}_{h_o}, \Theta_o) - \mu_{\Theta_o})\}}{\sigma_{\Theta_i}\sigma_{\Theta_o}} \tag{6}$$

On the other hand, it has been indicated in [8], and it will also be justified later, that the first and second order characteristics of the shadowing statistics, the mean and standard deviation, show a very slight variation with tilt that the overall shadowing map has closely the same statistical distribution before and after tilt change. Hence, it is reasonable to assume the same value of shadowing standard deviation at various tilt, i.e. $\sigma_{\Theta_i} \approx \sigma_{\Theta_o}$. According to the ray tracing based propagation data, the shadowing effect variability and statistical de-correlation of the shadowing values at $\overline{x}_{h_o}$ for different tilt increases with the amount of $\Delta\Theta$ applied. This in turn leads to an increase in the standard deviation $\sigma_{\Delta S}$ of $\Delta S(\overline{x}_{h_o}, \Theta_i, \Theta_o)$.

The tilt dependent shadowing model proposes a prediction approach to find a shadowing map $\hat{S}(\overline{x}_{h_o}, \Theta_i)$ for Θ_i tilt configuration from a known shadowing map at a reference tilt Θ_o. In our investigation, $\hat{S}(\overline{x}_{h_o}, \Theta_i)$ is to be predicted accordingly from the $S(\overline{x}_{h_o}, \Theta_o)$ statistics which is extracted from the ray tracing propagation map data generated at a tilt of Θ_o. In this case, the proposed model should also maintain the statistical correlation level observed between the extracted shadowing values at Θ_i and Θ_o tilt settings. Hence, a cross correlation coefficient $\hat{\rho}^{\Theta_i\Theta_o}$ is defined to give the statistical correlation level between the predicted shadowing statistics at Θ_i with the reference shadow map at Θ_o. In order to estimate $\hat{\rho}^{\Theta_i\Theta_o}$, the proposed model introduces a correlation coefficient predictor function $f_s(\Delta\Theta)$ that approximates the corresponding correlation level between two shadowing statistics for tilt setting difference $\Delta\Theta$,

$$\hat{\rho}^{\Theta_i\Theta_o} = f_s(\Delta\Theta) \tag{7}$$

where $f_s(\Delta\Theta)$ is going to be derived empirically by using ray tracing based extracted tilt dependent shadowing statistics from a real world based 3D deployment scenario, from several sectors. It has been observed in [8] and it will be also shown in later section that the cross correlation coefficient values drop linearly with $\Delta\Theta$. As a result, the function $f_s(\Delta\Theta)$ can be approximated as a linear predictor function with coefficients a and b such that $f_s(\Delta\Theta) = a \cdot \Delta\Theta + b$. The coefficients a and b are to be determined empirically based on the cross correlation coefficient data values $\rho^{\Theta_i\Theta_o}$ found from the ray tracing propagation map data extracted shadowing statistics.

During the tilt change of $\Delta\Theta$, the proposed model estimates the shadowing effect $\hat{S}(\overline{x}_{h_o}, \Theta_i) \sim \mathcal{N}(0, \hat{\sigma}_{\Theta_i}^2)$ at $\Theta_i = \Theta_o + \Delta\Theta$ from the shadowing value before the tilt change $S(\overline{x}_{h_o}, \Theta_o)$ and an additional uncorrelated Gaussian random variable $\Omega(\Delta\Theta) \sim \mathcal{N}(0, \sigma_{\Omega}^2)$. Utilizing the predicted cross correlation coefficient $\hat{\rho}^{\Theta_i\Theta_o}$, the resulting shadowing is modeled as:

$$\hat{S}(\overline{x}_{h_o}, \Theta_i) = \hat{\rho}^{\Theta_i\Theta_o} \cdot S(\overline{x}_{h_o}, \Theta_o) + \sqrt{1 - \hat{\rho}^{\Theta_i\Theta_o}} \cdot \Omega(\Delta\Theta) \tag{8}$$

where:

$$\hat{\rho}^{\Theta_i \Theta_o} = \frac{\text{Exp}\{(\hat{S}(\overline{x}_{h_o}, \Theta_i) - \hat{\mu}_{\Theta_i})(S(\overline{x}_{h_o}, \Theta_o) - \mu_{\Theta_o})\}}{\sigma_{\Theta_i} \sigma_{\Theta_o}} = f_s(\Delta \Theta) \tag{9}$$

As discussed earlier, $\hat{\sigma}_{\Theta_i} \approx \sigma_{\Theta_o}$. Thus, σ_{Ω} can be derived from the variance relationship as:

$$\text{Var}[\hat{S}(\overline{x}_{h_o}, \Theta_i)] = \text{Var}[S(\overline{x}_{h_o}, \Theta_o)] \tag{10}$$

$$\text{Var}[\hat{\rho}^{\Theta_i \Theta_o} \cdot S(\overline{x}_{h_o}, \Theta_o) + \sqrt{1 - \hat{\rho}^{\Theta_i \Theta_o}} \cdot \Omega(\Delta \Theta)] = \sigma_{\Theta_o}^2 \tag{11}$$

From the above expression the σ_{Ω} is:

$$\sigma_{\Omega} = \sqrt{1 + \hat{\rho}^{\Theta_i \Theta_o}} \cdot \sigma_{\Theta_o} \tag{12}$$

Accordingly, the total propagation loss $\hat{L}_t(\overline{x}_{h_o}, \Theta_i)$ expression at Θ_i shown in Eq. (5) can be rewritten by including the predicted shadowing effect change $\Delta \hat{S}(\overline{x}_{h_o}, \Theta_i, \Theta_o)$ as,

$$\hat{L}_t(\overline{x}_{h_o}, \Theta_i) = L_t(\overline{x}_{h_o}, \Theta_o) + \Delta G_a(\overline{x}_{h_o}, \Theta_i, \Theta_o) + \Delta \hat{S}(\overline{x}_{h_o}, \Theta_i, \Theta_o) \tag{13}$$

where:

$$\Delta \hat{S}(\overline{x}_{h_o}, \Theta_i, \Theta_o) = \hat{S}(\overline{x}_{h_o}, \Theta_i) - S(\overline{x}_{h_o}, \Theta_o) \tag{14}$$

$$\Delta \hat{S}(\overline{x}_{h_o}, \Theta_i, \Theta_o) = (\hat{\rho}^{\Theta_i \Theta_o} - 1) \cdot S(\overline{x}_{h_o}, \Theta_o) + \sqrt{1 - \hat{\rho}^{\Theta_i \Theta_o}} \cdot \Omega(\Delta \Theta) \tag{15}$$

The standard deviation of $\Delta \hat{S}(\overline{x}_{h_o}, \Theta_i, \Theta_o)$, $\hat{\sigma}_{\Delta S}$, can be found by evaluating the variance of equation above and using the relationship shown in above, and it becomes:

$$\hat{\sigma}_{\Delta S} = \sqrt{2 \cdot (1 - \hat{\rho}^{\Theta_i \Theta_o})} \cdot \sigma_{\Theta_o} \tag{16}$$

3.2 Height Gain Model

In this paper the height gain effect is investigated by means of evaluating the floor height gain values from propagation maps generated at different floor height levels using the employed ray tracing tool. The investigation aims at showing the statistical variation of the floor height gains and compares it with the existing constant average hight gain assumption of 0.6 dB/m [10]. In reality this constant gain value deviates randomly depending on the type of propagation environment. Hence, the proposed height gain model approximates the effect of the clutter type with a better estimation of height gain values.

Accordingly, a non constant and variable height gain denoted by $\hat{H}(\overline{x}_{h_i, h_o})$ is determined by subtracting the ray tracing propagation map generated at h_i and h_o floor height levels. Thus, the total propagation loss $\hat{L}_t(\overline{x}_{h_i}, \Theta_o)$ at h_i height level can now be rewritten as:

$$\hat{L}_t(\overline{x}_{h_i}, \Theta_o) = L_t(\overline{x}_{h_o}, \Theta_o) + \hat{H}(\overline{x}_{h_i, h_o}) \tag{17}$$

where $\hat{H}(\overline{x}_{h_i, h_o}) = \hat{L}_t(\overline{x}_{h_i}, \Theta_o) - L_t(\overline{x}_{h_o}, \Theta_o)$ gives the corresponding floor height gain. The height gain model in this paper investigates the statistical variation of $\hat{H}(\overline{x}_{h_i, h_o})$ and compares it with the existing model assumption by utilizing the ray tracing based propagation map statistics generated for a multi-floor scenario in Sect. 5.
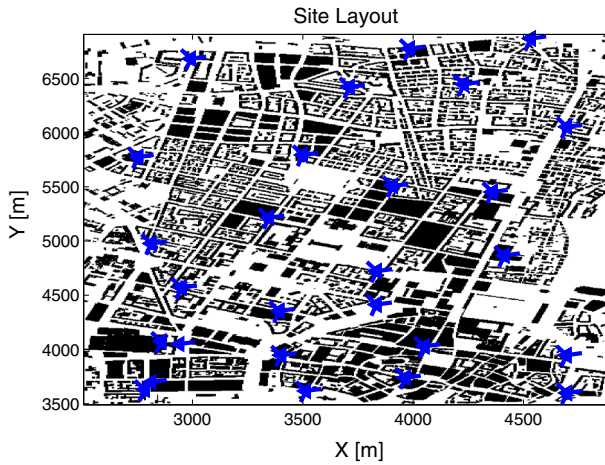
Fig. 2 Ray tracing site layout

4 Ray Tracing Scenario Description and Statistics Extraction

4.1 Ray Tracing Scenario

For the investigation, a network planning tool that employs ray tracing technique for the propagation map prediction is used. A 3D city model and the urban clutter behavior of a typical European city is considered in the scenario. The scenario assumes 27 sectorized sites consisting of 75 sectors where the site plan and system parameter configuration settings are done based on realistic site deployment information. In the ray tracing tool, Dominant path Prediction Model (DPM) is adopted where the propagation loss from a transmitting antenna to a point is predicted in the direction of a ray path taken by the dominant ray which brings most of the energy to the point of prediction. It has been shown in [11,12] that DPM has as high accuracy as the prediction technique that employs several rays. The ray tracing technique along with the 3D models reflects the real propagation effects and an accurate prediction of the received signal at each pixel point. The propagation prediction is done for each sector antenna in a pixel based approach where the total network is divided into a grid of pixels of 5 m resolution with a total prediction area of 3.4 km by 2.4 km. The site layout and the prediction area of the ray tracing scenario is shown in Fig. 2 and basic system parameters settings are also summarized in Table 1.

Two sets of outdoor propagation maps are generated via ray tracing based prediction of the received signal strength at each pixel point from each sector antenna. One set of prediction is done for ground floor at a 1.5 m user height level for different tilt settings varying from 4° to 14° in order to carry out the tilt dependent shadowing investigation. The other set of prediction has been carried out at different floor height levels but fixed tilt setting for the height gain study. The indoor propagation is estimated from the outdoor maps by adding a 10 dB penetration loss plus an additional attenuation of 0.6 dB/m to the strongest ray detected around the building being considered [9,10,13].

4.2 Statistics Extraction

The total propagation loss $L_t(\overline{x}_{h_i}, \Theta_i)$ map is obtained by subtracting the total transmit power level used in the prediction, i.e. 43 dBm, from the generated received power map. The

Table 1 Basic scenario settings

Information	Settings
Network size	3.4 km by 2.4 km
Site and sector	27 sites, 75 sectors
Transmit power	20 W (43 dBm)
Antenna gain	17.5 dBi
Radiation beam	$\Phi_{3dB} = 62$, $\Theta_{3dB} = 5$
Sector orientation	[10°, 250°, 130°]
Mechanical tilt	4°
Electrical tilt	0°–10°, step 1°
Prediction height	Ground + 6 Floor
Floor height	3.1 m
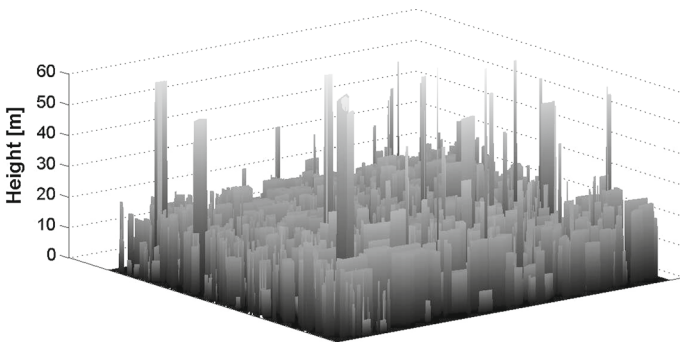
Fig. 3 3D city building layout used in ray tracing scenario

corresponding shadowing maps are extracted for each prediction setting scenario of Θ_i tilt and h_i m height by using the empirical propagation model described in Eq. (2). Accordingly, $S(\overline{x}_{h_i}, \Theta_i)$ is given as:

$$S(\overline{x}_{h_i}, \Theta_i) = L_t(\overline{x}_{h_i}, \Theta_i) - L(\overline{x}_{h_i}) + G_a(\overline{x}_{h_i}, \Theta_i). \quad (18)$$

Since only $L_t(\overline{x}_{h_i}, \Theta_i)$ is available from Eq. (18), the path loss component $L(\overline{x}_{h_i})$ and the total antenna gain $G_a(\overline{x}_{h_i}, \Theta_i)$ values are needed to be determined. It is apparent that $L(\overline{x}_{h_i})$ is the mean propagation loss whereas the $S(\overline{x}_{h_i}, \Theta_i)$ corresponds to the rest of the large scale attenuation over the mean, thus, the path loss plus shadowing can be evaluated from Eq. (18) as:

$$S(\overline{x}_{h_i}, \Theta_i) + L(\overline{x}_{h_i}) = L_t(\overline{x}_{h_i}, \Theta_i) + G_a(\overline{x}_{h_i}, \Theta_i) \quad (19)$$

In this case, the path loss is approximated by the empirical path loss model as $L(\overline{x}_{h_i}) = \alpha + \beta \cdot \log_{10}(r)$ where α and β are the path loss loss coefficients and can be determined via linear regression estimation from the the path loss plus shadowing statistics and the coefficients correspond to the path loss offset and the path loss exponent, respectively [5,6].

Proper extraction of the shadowing statistics requires estimating and excluding of the total antenna gain values with respect to each $\overline{x}_{h_i}$ in Eq. (19). And this needs a beam pattern model that provides the antenna gain variation. In this investigation, the beam pattern model from 3rd Generation Partnership Project (3GPP) [6] is employed. The two dimensional and total three dimensional patterns are approximated as shown in Eqs. (20)–(22) where the variables
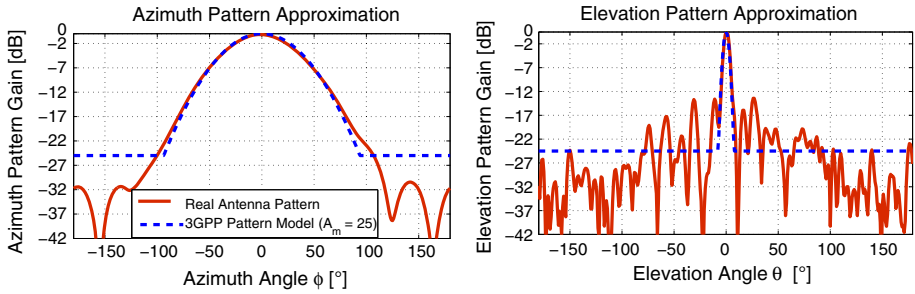
Fig. 4 Approximation of the real antenna radiation pattern

Φ_o, Θ_i, Φ_{3dB} and Θ_{3dB} are the azimuth orientation, elevation tilt, azimuth and elevation half power beam-widths, respectively [6,14], whereas ϕ and θ are the angular position of $\overline{x}_{h_i}$. The 3GPP pattern model estimates the main lobe radiation patterns and approximates the side and back lobe effect with a constant value of A_m known as backward attenuation factor. Figure 4 depicts the estimated and real antenna elevation pattern behaviour for a typical value of $A_m = 25$ dB proposed by 3GPP [6].

$$B_H(\phi) = - \min \left\{ A_m, 12 \cdot \left(\frac{\phi - \Phi_o}{\Phi_{3dB}} \right)^2 \right\}, \Rightarrow \text{Azimuth} \tag{20}$$

$$B_V(\theta) = - \min \left\{ A_m, 12 \cdot \left(\frac{\theta - \Theta_i}{\Theta_{3dB}} \right)^2 \right\} \Rightarrow \text{Elevation} \tag{21}$$

$$B_{3D}(\phi, \theta) = - \min \left\{ A_m, -\left[B_H(\phi) + B_V(\theta) \right] \right\}, \Rightarrow \text{Total Pattern} \tag{22}$$

However, the backward attenuation effect depends on the nature of the propagation environment as it attributes to the various physical phenomena that the signal wave undergoes during radiation like reflection, scattering and diffraction which determines the effective antenna gain behavior from side lobes [14,15]. As a consequence, A_m is characterized by the clutter type seen by each antenna and could have different values for each antenna in the same scenario. Hence, an exhaustive search optimization has been carried out for a range of A_m values that will lead to a path loss plus shadowing statistics satisfying a minimum standard deviation criteria for the shadowing [8].

## 5 Model Coefficient Prediction and Performance Evaluation

5.1 Shadowing Statistics and Predictor Coefficients

5.1.1 Shadowing Statistics

The shadowing statistics extracted for each tilt Θ_i from the ray tracing data, $S(\overline{x}_{h_o}, \Theta_i)$, has been investigated for its statistical behavior and invariability property along with the applied tilt change. Statistics observed from each site antenna confirmed that the extracted shadow map for each tilt settings have a Gaussian statistical distribution with closely the same standard deviation independent of the tilt. This is also illustrated in Fig. 5 where the shadowing map distribution is shown for a sample site for different tilt case validating that
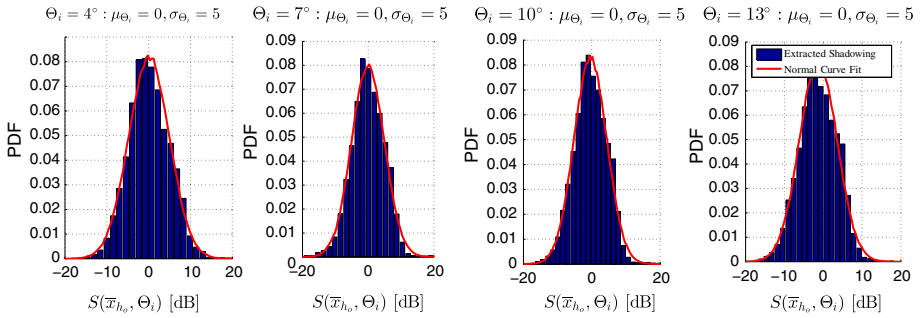
Fig. 5 Distribution of extracted Shadowing values, $S(\overline{x}_{h_o}, \Theta_i)$, for different Θ_i
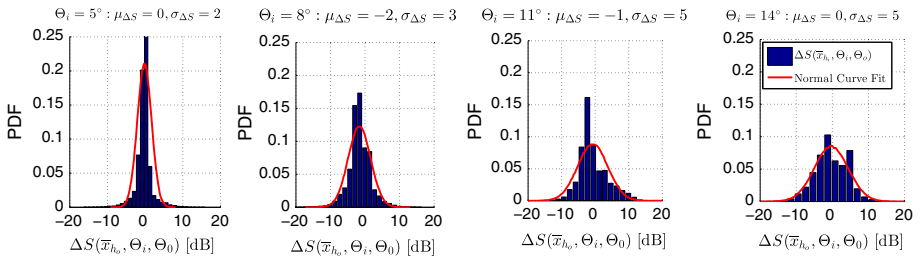
Fig. 6 Distribution of shadowing value differences, $\Delta S(\overline{x}_{h_o}, \Theta_i, \Theta_0)$, for different Θ_i

the standard deviation of the shadowing statistics is independent of the tilt change as assumed in Sect. 3.

However, this does not guarantee the invariability of the shadowing effect with respect to tilt change. Hence, further investigation is done by evaluating the corresponding shadowing map change, $\Delta S(\overline{x}_{h_o}, \Theta_i, \Theta_o)$, at each pixel $\overline{x}_{h_o}$ location in the prediction area for the applied tilt setting change. Figure 6 shows the distribution of the shadowing value differences $\Delta S(\overline{x}_{h_o}, \Theta_i, \Theta_o)$ for various tilt differences evaluated per pixel showing that the shadowing effect indeed changes while tilt setting is varied. The figure confirms that $\Delta S(\overline{x}_{h_o}, \Theta_i, \Theta_o)$ also follows a Gaussian distribution with a mean value around zero and standard deviation, $\sigma_{\Delta S}$, which is increasing with $\Delta\Theta$ indicating that the actual shadowing experience has dependency on the tilt and the shadowing effect variation gets higher at a larger relative tilt change. Moreover, the statistical mean and standard deviation of the shadowing map are not changed considerably with tilt as discussed before and this behavior is more depicted in Fig. 7 for various tilt Θ_i.

5.1.2 Shadowing Correlation and Predictor Coefficients

Shadow fading effects at different locations depend on the transmitting base station location with respect to the receiver terminal and the surrounding environment of the considered pixel location. Shadowing values of the neighboring pixels exhibit a statistical correlation which is also used in the existing shadowing model for system level simulations in order to generate a shadowing map with respect to each site [6]. In this investigation, the statistical correlation property among shadowing map associated for different tilt settings is exploited in order to derive the relationship between the random shadowing process at different tilt settings.
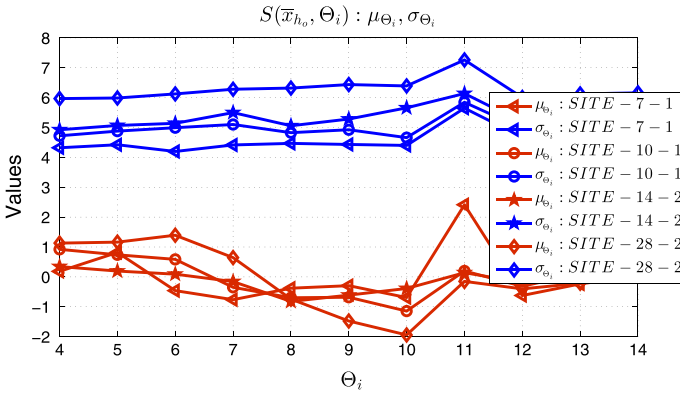
Fig. 7 Mean and standard deviation of $S(\overline{x}_{h_o}, \Theta_i)$ at different Θ_i
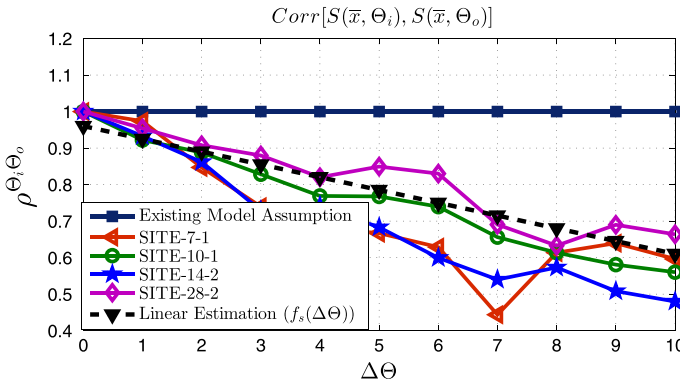

Fig. 8 Shadowing correlation coefficients for various $\Delta\Theta$

In the existing shadowing model [6], since the same shadowing effect is assumed irrespective of the tilt setting, the random shadowing process is seen as fully correlated before and after a tilt change. In reality, however, the shadowing statistics extracted from the ray tracing propagation map data for different tilt settings show that the shadowing fading effect for any two different tilt settings does not remain the same and the variation increases with the increase in the tilt difference. This is illustrated in Fig. 8 where the shadowing correlation coefficient value is shown for the shadowing at a reference tilt, $\Theta_o = 4°$, and at a different tilt settings, Θ_i. This confirms the existence of tilt dependency of the shadowing fading with respect to the antenna tilt setting. The figure also depicts that the shadowing correlation level drops approximately linearly with the applied tilt change.

As discussed in Sect. 3, the new model introduced in this paper defines a linear function, $f_s(\Delta\Theta)$ as shown in Eq. (23), to predict the corresponding statistical correlation level of the shadowing effect at, $\hat{\rho}^{\Theta_i\Theta_o}$, for a tilt change of $\Delta\Theta$ from Θ_o to Θ_i. The coefficients of $f_s(\Delta\Theta)$ are determined from the shadowing correlation coefficients, $\rho^{\Theta_i\Theta_o}$, evaluated from the ray tracing based shadowing statistics for various tilt settings using a linear curve fitting approach as shown in Fig. 8. The linear predictor function is given by Eq. (23) with coefficients a and b.

$$\hat{\rho}^{\Theta_i\Theta_o} = f_s(\Delta\Theta) = a \cdot \Delta\Theta + b \tag{23}$$

The approximation of predictor coefficients is done using a linear least square method such that $f_s(\Delta\Theta)$ fits the correlation coefficient data, $\rho_{k,i}^{\Theta_i\Theta_o}$, calculated from each sector k for different tilt change values, $\Delta\Theta_i$, at N number of sectors in our ray tracing scenario where $\Delta\Theta_i = \Theta_i - \Theta_o$. In this investigation, 19 sectors are randomly considered and at each sector, the tilt configuration, Θ_i, is changed from $4°$ up to $14°$ with $1°$ step size resulting in $T = 11$ tilt settings. Thus, the coefficients a and b that linearly best fit the data minimizing the error ϵ in Eq. (24) are calculated accordingly.

$$\epsilon = \sum_{k=1}^{N}\sum_{i=1}^{T}(\rho_{k,i}^{\Theta_i\Theta_o} - (a \cdot \Delta\Theta_i + b))^2 \tag{24}$$

Thus, based on the shadowing values extracted from the ray tracing based generated propagation maps, predictor coefficient value of $a = -0.035$ and $b = 0.96$ are found with error $\epsilon = 2.3$. The correlation coefficient predictor function is then given by $f_s(\Delta\Theta) = -0.035 \cdot \Delta\Theta + 0.96$ and its slop indicates that the shadowing correlation drops by approximately 3% per $1°$ tilt change.

5.1.3 Performance of the Proposed Model

In this subsection the performance of the proposed model is checked against the ray tracing data. In this case, a new shadowing map of $\hat{S}(\overline{x}_{h_o}, \Theta_i)$ is generated for a sector at a tilt setting Θ_i from the ray tracing propagation extracted shadowing map $S(\overline{x}_{h_o}, \Theta_o)$ of the same sector at the reference tilt, $\Theta_o = 4°$, by using the proposed model described in Eqs. (7)–(15) and the correlation coefficient predictor function. The statistical correlation between the predicted $\hat{S}(\overline{x}_{h_o}, \Theta_i)$ and $S(\overline{x}_{h_o}, \Theta_o)$ is equal to $\hat{\rho}^{\Theta_i\Theta_o}$ and it is the same as the value of $f_s(\Delta\Theta)$ evaluated for the respective tilt change. Thus, the correlation property is well approximated by the model as already demonstrated in Fig. 8. The mean $\hat{\mu}_{\Theta_i}$ and the standard deviation $\hat{\sigma}_{\Theta_i}$ of the newly generated shadowing map, $\hat{S}(\overline{x}_{h_o}, \Theta_i)$, at different tilt setting is also evaluated for selected sites. The standard deviation of the normally distributed random values, $\Omega(\Delta\Theta)$, used while generating $\hat{S}(\overline{x}_{h_o}, \Theta_i)$ is also determined as described in Eq. (11) and in this case it is also assumed that independent random values are generated for pixel points separated by the same de-correlation distance as $S(\overline{x}_{h_o}, \Theta_0)$ and the other values in between are evaluated via interpolation. Spatial de-correlation distance of 40 m is assumed in our case during generating the new shadowing map while validating the performance of the proposed model.

Results shown in Fig. 9 have indicated that the $\hat{S}(\overline{x}_{h_o}, \Theta_i)$ has closely the same statistical distribution with the shadowing map $S(\overline{x}_{h_o}, \Theta_i)$ extracted from the ray tracing data. This is illustrated by comparing the corresponding mean and standard deviation values for the extracted and the newly generated shadow map depicted in Figs. 7 and 9 respectively at different tilt settings.

Moreover, it is also interesting to show how close the model predicts the corresponding shadowing effect change, $\Delta\hat{S}(\overline{x}_{h_o}, \Theta_i, \Theta_o)$, that happens during the tilt configuration change from Θ_i to Θ_o which is found by subtracting the shadowing values at each pixel, $\overline{x}_{h_o}$, at the respective tilt settings, i.e. $\Delta\hat{S}(\overline{x}_{h_o}, \Theta_i, \Theta_o) = \hat{S}(\overline{x}_{h_o}, \Theta_i) - S(\overline{x}_{h_o}, \Theta_o)$. Thus, this value is checked with the corresponding shadowing difference values evaluated from the ray tracing data at the respective tilt settings, i.e. $\Delta S(\overline{x}_{h_o}, \Theta_i, \Theta_o) = S(\overline{x}_{h_o}, \Theta_i) - S(\overline{x}_{h_o}, \Theta_o)$. The comparison between distribution curves and standard deviation values shown in Figs. 6 and 10 demonstrate that the proposed model predicts the shadowing variation with respect tile changes closely to what is observed from the ray tracing data.
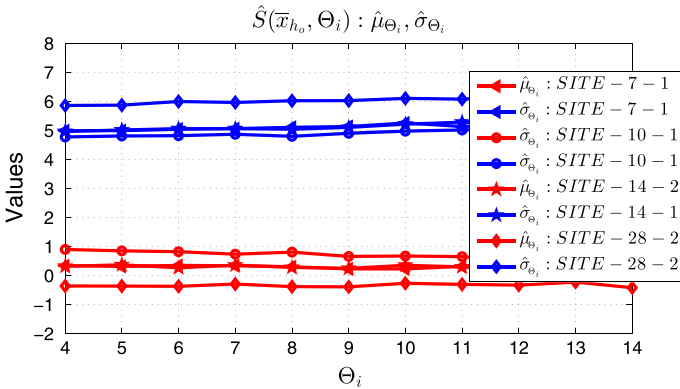
$$\hat{S}(\overline{x}_{h_o}, \Theta_i) : \hat{\mu}_{\Theta_i}, \hat{\sigma}_{\Theta_i}$$

Fig. 9 Mean and standard deviation of $\hat{S}(\overline{x}_{h_o}, \Theta_i)$ at different Θ_i
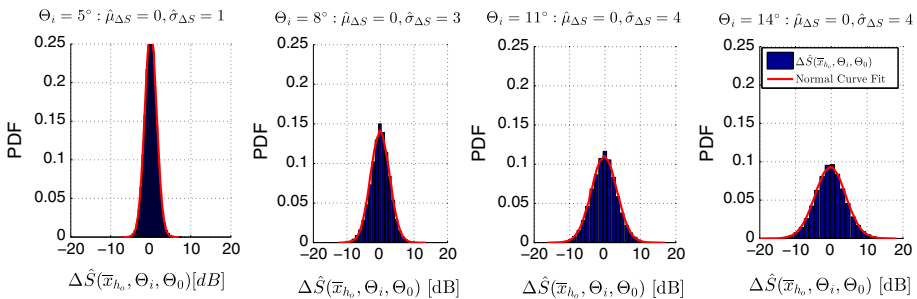

Fig. 10 $\Delta\hat{S}(\overline{x}_{h_o}, \Theta_i, \Theta_0)$ statistical distribution

5.2 Statistical Behavior of Height Gain

The height gain effect is investigated by using the propagation maps generated by a ray tracing tool for the considered 3D urban model scenario depicting a typical European city clutter type as shown in Fig. 3. In this case the total propagation loss $L(\overline{x}_{h_i}, \Theta_o)$ is predicted at a different floor height level using ray tracing technique where the ray tracing tool considers the propagation effects experienced in real life by using the employed 3D model scenario during the propagation map prediction. Accordingly, various propagation maps are generated for 7 different floors at a different height levels, i.e. ground floor at 1.5 m hight and 6 higher floors with 3.1 m height difference between them.

Accordingly, the height gain $\hat{H}(\overline{x}_{h_i, h_0})$ at each pixel points $\overline{x}$ at a floor height level of h_i with respect to the ground floor height h_o is evaluated from the ray tracing propagation maps, predicted for each floor height, as shown in Eq. (25).

$$\hat{H}(\overline{x}_{h_i, h_0}) = L(\overline{x}_{h_i}, \Theta_o) - L(\overline{x}_{h_o}, \Theta_o); \quad (25)$$

The evaluated $\hat{H}(\overline{x}_{h_i, h_0})$ statistics from each pixel points are analyzed for different sectors. $\hat{H}(\overline{x}_{h_i, h_0})$ statistical distribution is presented in Fig. 11 for one sample sector from the ray tracing scenario. It can be seen from the figure that, the height gain value is different at different location and this value even deviates significantly from the corresponding average height gain value at the respective floor height level. The deviation is due to the fact that the clutter effect experienced at various points at a certain floor height level is different at different
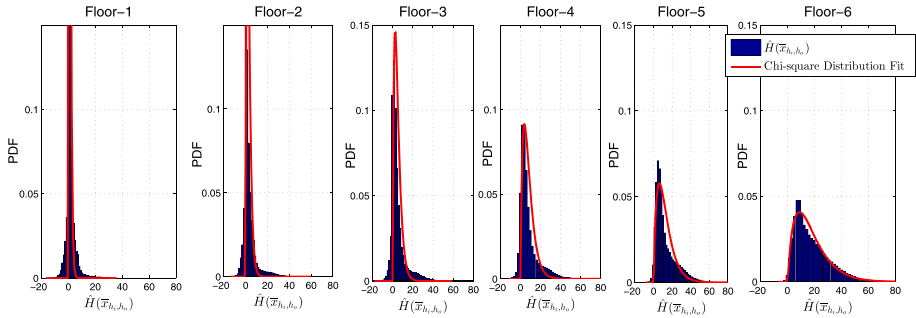
Fig. 11 $\hat{H}(\overline{x}_{h_i,h_0})$ statistical distribution with respect to the ground floor
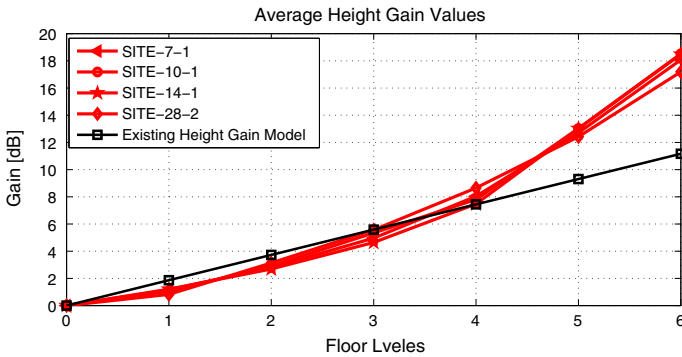

Fig. 12 Average floor height gain value comparisons for different floors

building locations. The average floor height gain level is also evaluated for various sector propagation cases and it is compared with the exiting 0.6 dB/m gain in Fig. 12. The same kind of statistical distribution behavior is observed for the height gain values evaluated with respect to different sectors. It has been also shown in Fig. 11 that the height gain statistics follows a chi-square distribution and fits well in the figure with a chi-square distribution curve with 4 degree of freedom, i.e. $\hat{H}(\overline{x}_{h_i,h_0}) \sim \chi_4^2$, centered at different mean for each floor height level.

As it can be seen in Fig. 12, the average height gain values extracted from the ray tracing data fits quite well until the 4th floor but different starting higher floors. This could be attributed to the specific clutter type considered in our ray tracing 3D urban scenario. However, the average height gain from different sites shows quite similar trends.

6 Impact of Tilt and Height Based Models in Network Planning and Optimization

The proposed tilt dependent shadowing model and the floor height gain investigation results have shown that proper tuning is required to the existing propagation model in order to accurately reflect the real time propagation effects. As discussed in the Sect. 2, in network planning and optimization tasks, the planning and optimization tool should be able to properly estimate the accompanying changes that occurs in reality due to any applied change in network parameters. The antenna tilt is one of the significant radio parameters

Fig. 13 RSRP CDF from ray tracing scenario for different floor height
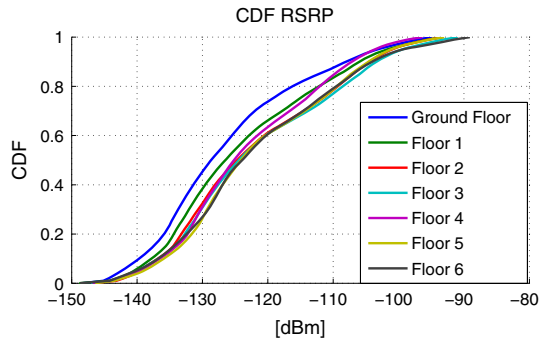
which is used in order to ensure network coverage and also to control the co-channel inter-ference level in the system. In dynamic and flexible cell lay out deployment, supported by the AAS features, the antenna beam orientation is adapted to the capacity and traffic demands in the network. Evaluation phases of a self-organized network operation mecha-nisms and algorithms as well as network planning tools should include the impact of the tilt change and the corresponding clutter type variation experienced in the course of radio signal propagation.

In the case of multi-floor building scenario, using a constant floor height gain, as proposed by the existing model, always leads to a propagation gain that increases linearly with floor height level as depicted in Fig. 12. However, in reality, the floor height gain value is highly dependent on the relative position of a user location with respect to the corresponding trans-mitting antenna and also the line of sight probability for the signal reception at respective floor height level. Consequently, the height gain value might not be observed despite an increase in floor height level if the clutter effect remains unchanged. Figure 13 illustrates the height gain trends with the Cumulative Distribution Function (CDF) of the Reference Signal Received Power (RSRP) level evaluated for indoor propagation at various floors taken from the ray tracing scenario. From the figure, it can be seen that, the floor height gain is observed up to the 3rd floor while no height gain is observed at higher percentiles. At the lower percentile of the CDF curve, it can also be seen that the height gain is observed up to a certain floor level and stops showing further gain while increasing the floor level. This is due to the fact that, the line of sight probability and the clutter experience of some locations gets worse with height due to their geographical location with respect the transmitting antenna. The presence of various height gain experience in real network results in a different RSRP level reception at each floor height but different locations. This, consequently, leads to a different cell coverage and serving cell dominance per floor.

According to the the existing floor height gain model, however, the signals received from any transmitting antenna will have the same amount of height gain, therefore, the existing model predicts the same server map plot for each floor at any 2D location, $\bar{x}$. However, the best server map plots found from the ray tracing data which are shown in Fig. 14 demonstrates that, due to the random variation of the height gain values, certain locations could experience different floor height gains on the RSRP value detected from different transmitting sector antennas. As a consequence, users could lie under different best server sector coverage at the same 2D geographical location while being at different floor heights. It is also well illustrated in Fig. 14 that while changing the floor, a new sector could merge and dominate a certain coverage area. Other sectors also change either the size of their coverage dominance area or disappear after a certain floor.
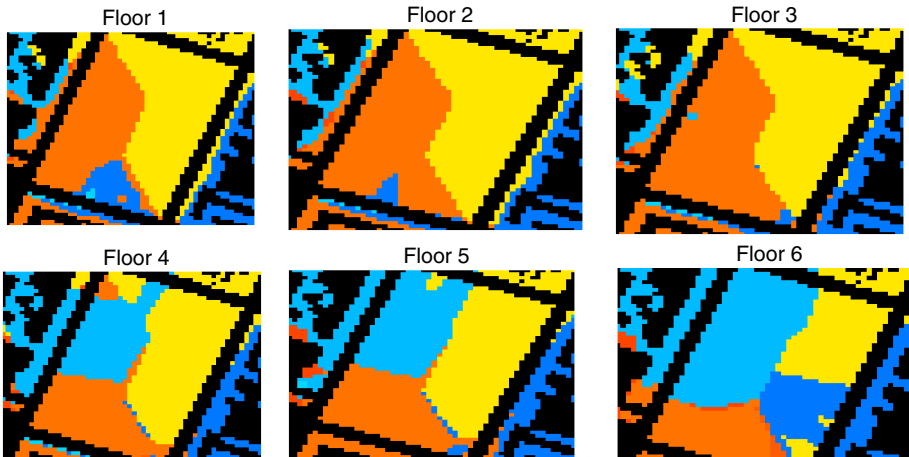
**Fig. 14** Best server map plot at different floor levels

7 Conclusion

In this paper, a new tilt dependent shadowing model is proposed as an extension to the existing propagation shadowing model. The tilt dependent shadowing model predicts the shadowing effect variation that could be experienced in real propagation environment when a tilt configuration change is applied. While the tilt is changed, the proposed model approximates and generates new shadowing fading values from the shadowing effect assumed before the tilt change. The level of the change in the shadowing effect with the tilt difference and the corresponding de-correlation of the shadowing process can be also predicted by the proposed shadowing model. The model is derived and validated with a ray tracing based generated propagation maps for a 3D model scenario of a typical European city urban clutter type. Though sample site results are presented in the paper, the investigation has been carried out for 75 different sectors and closely the same prediction performance is observed in the proposed model.

Furthermore, the floor height gain variation and its effects have been investigated and discussed in this paper. It has been found out that the height gain variation deviates from the mean value with an increase in height level. Moreover, ray tracing based data has demonstrated that the floor height gain is actually different for different locations and hence, in real deployment, it leads to a different server map experience for a service area depending on the pixel relative location with respect to the transmitting antenna. This suggests to use a random variable floor height gain than a deterministic gain value as stated in the existing model.

The proposed tilt dependent model is derived based on the propagation map data generated using a ray tracing tool considering a typical urban scenario. Hence, some parameter values introduced in the proposed model might be scenario dependent, for example, the correlation prediction function $f_s(\Delta\Theta)$ whose coefficients are derived from the considered specific scenario. Therefore, universal application of the proposed shadowing model still requires analysis with different various scenarios. The authors would like to put this limitation as an outlook in order to investigate how far the predictor coefficients deviate from one scenario to another scenario.

References

1. Walfisch, J., & Bertoni, H. L. (1988). A theoretical model of UHF propagation in urban environments. *IEEE Transactions on Antennas and Propagation*, *36*(12), 1788–1796.
2. Ikegami, F., Yoshida, S., Umehira, M., & Takeuchi, T. (2003). Propagation factors controlling mean field strength on urban streets. *IEEE Transactions on Antennas and Propagation*, *36*(8), 317–325.
3. Hata, M. (1980). Empirical formula for propagation loss in land mobile radio services. *IEEE Transactions on Vehicular Technology*, *29*(3), 822–829.
4. Cichon, D. J., & Kürner, T. (1999). Propagation prediction models. COST Telecommunications Action 231 Final Report, COST Telecom Secretariat, Commission of the European Communities, Brussels, Belgium, pp. 117–195.
5. Stüber, G. (2011). *Principles of mobile communication* (3rd ed.). Springer New York Dordrecht Heidelberg London: Springer.
6. 3GPP. (2006). Evolved universal terrestrial radio access (E-UTRA); Further advancements for (E-UTRA) Physical layer aspect, 3rd Edition. TR 36.814, 19–21.
7. Yilmaz, O., Hämäläinen, S., & Hämäläinen, J. (2009). System level analysis of vertical sectorization for 3GPP LTE: 6th International Symposium on Wireless Communication Systems. *ISWCS*, *2009*, 453–457.
8. Kifle, D. W., Wegmann, B., Viering, I., & Klein, A. (2013). Impact of antenna tilting on propagation shadowing model. *IEEE 77th Vehicular Technology Conference* (VTC Spring).
9. Okamoto, H., Kitao, K., & Ichitsubo, S. (2009). Outdoor-to-indoor propagation loss prediction in 800-MHz to 8-GHz band for an urban area. *IEEE Transactions on Vehicular Technology*, *58*(3), 1059–1067.
10. Berg, J. E. (1999). Propagation Prediction Models (building penetration). COST Telecommunications Action 231 Final Report, COST Telecom Secretariat, Commission of the European Communities, Brussels, Belgium, pp. 167–174.
11. Wölfle, G., Wahl, R., Wildbolz, P., & Wertz, P. Dominant path prediction model for indoor and urban scenarios. AWE Communications, Tech. Rep.
12. Burger, S. (2003). *Accuracy of winprop 3D intelligent ray tracing: AWE Communications*. Tech. Rep.
13. Rappaport, T. S., & Sandhu, S. (1994). Radio-wave propagation for emerging wireless personal-communication systems. *IEEE Antennas and Propagation Magazine*, *36*(5), 14–24.
14. Giland, F., Claro, A., Ferreira, J., Pardelinha, C., & Correia, L. (2001). A 3D interpolation method for base-station-antenna radiation patterns. *IEEE Antennas and Propagation Magazine*, *43*(2), 132–137.
15. Huemer, E., & Lensing, K. (2000). *Practical antenna guide*. KATHREIN MOBILCOM BRASIL Ltda, Tech. Rep.
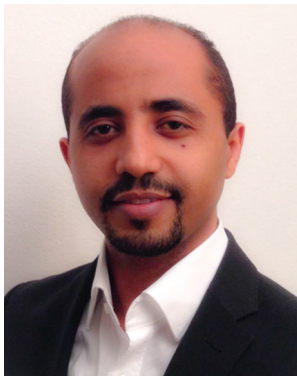
Dereje W. Kifle received his B.Sc. degree in Electrical Engineering from Bahir Dar University, Bahir Dar, Ethiopia in 2007. From 2007 to 2009, he worked as a staff member in the Electrical and Computer Engineering Department of Bahir Dar University Engineering Faculty. In 2009, he joined University of Trento, Trento, Italy, and received his M.Sc. degree in Telecommunications Engineering in 2011 from University of Trento. He is currently working toward his PhD with the Department of Communication Technology at Technical University of Darmstadt, Darmstadt, Germany. Since 2011, he has been conducting his research activities in the Department of Radio Systems in former Nokia Siemens Networks, now Nokia Networks, Munich, Germany. His research activities and interests include Propagation Modeling, Network Deployment Automation and Optimization.

Lucas C. Gimenez obtained his M.Sc. in Mobile Communications from Aalborg University in 2011. He is currently pursuing the PhD degree in wireless communications at the Department of Electronic Systems at the same university. From 2012 to 2013, he has been employed as a research assistant at the Radio Access Technology Section from the Department of Electronic Systems at Aalborg University in collaboration with Nokia. His current research interests include mobility management in next-generation mobile networks.

Bernhard Wegmann received his Dipl.-Ing. and Dr.-Ing. (Ph.D.) degrees in 1987 and 1993 from University of Technology Munich, Germany. He is currently with Nokia Networks in Munich, Germany, where he is working as research manager for future mobile radio systems dealing with radio access enhancements for selforganizing networks in context of Long-Term Evolution (LTE) and LTE-Advanced technology. He is author/co-author of more than 50 technical publications and patent filings. His professional interests are on radio transmission techniques, radio resource management, self-organizing networks, and radio network deployment.

Ingo Viering is co-founder and CEO of Nomor Research GmbH located in Munich, Germany. Furthermore, since 2007 he is also senior lecturer at Munich University of Technology. His research interests are the system aspects of current and future communication systems including the detailed interaction of the multitude of features. Ingo got his Dr.-Ing. from University of Ulm in 2003. He spent a research stay with the "Telecommunications Research Center Vienna (FTW)" in 2002, where he conducted early measurements of the MIMO channel. He received his Dipl.-Ing. degree from the University of Technology Darmstadt in 1999. He has filed around 100 patents, published more than 70 scientific papers, and he is actively contributing to 3GPP. In 2009, he was awarded the VDE Award for the achievements of Nomor Research.

Anja Klein received the diploma and Dr.-Ing. (Ph.D.) degrees in electrical engineering from the University of Kaiserslautern, Germany, in 1991 and 1996, respectively. From 1991 to 1996, she was a member of the staff of the Research Group for RF Communications at the University of Kaiserslautern. In 1996, she joined Siemens AG, Mobile Networks Division, Munich and Berlin. She was active in the standardization of third generation mobile radio in ETSI and in 3GPP, for instance leading the TDD group in RAN1 of 3GPP. She was vice president, heading a development department and a systems engineering department. In May 2004, she joined the Technische Universität Darmstadt, Germany, as full professor, heading the Communications Engineering Lab. Her main research interests are in mobile radio, including multi-antenna systems, radio resource management, interference management, relaying and multi-hop, cooperative communication, network planning, and cross-layer design. Dr. Klein has published over 270 refereed papers and has contributed to ten books. She is inventor and co-inventor of more than 45 patents in the field of mobile radio. In 1999, she was inventor of the year of Siemens AG. Dr. Klein is a member of IEEE and of Verband Deutscher Elektrotechniker - Informationstechnische Gesellschaft (VDE-ITG).